JOM, Vol. 70, No. 2, 2018
DOI: 10.1007/s11837-017-2636-8

TECHNICAL COMMUNICATIONS

Computational Fluid Dynamics-Population Balance Model Simulation of Effects of Cell Design and Operating Parameters on Gas–Liquid Two-Phase Flows and Bubble Distribution Characteristics in Aluminum Electrolysis Cells

SHUIQING ZHAN,[1] JUNFENG WANG,[1,3] ZHENTAO WANG,[1] and JIANHONG YANG[2]

1.—School of Energy and Power Engineering, Jiangsu University, Zhenjiang 212013, People's Republic of China. 2.—School of Material Science and Engineering, Jiangsu University, Zhenjiang 212013, People's Republic of China. 3.—e-mail: wangjunfeng@ujs.edu.cn

The effects of different cell design and operating parameters on the gas–liquid two-phase flows and bubble distribution characteristics under the anode bottom regions in aluminum electrolysis cells were analyzed using a three-dimensional computational fluid dynamics-population balance model. These parameters include inter-anode channel width, anode–cathode distance (ACD), anode width and length, current density, and electrolyte depth. The simulations results show that the inter-anode channel width has no significant effect on the gas volume fraction, electrolyte velocity, and bubble size. With increasing ACD, the above values decrease and more uniform bubbles can be obtained. Different effects of the anode width and length can be concluded in different cell regions. With increasing current density, the gas volume fraction and electrolyte velocity increase, but the bubble size keeps nearly the same. Increasing electrolyte depth decreased the gas volume fraction and bubble size in particular areas and the electrolyte velocity increased.

INTRODUCTION

During the aluminum electrolysis process, the anodic bubbles are mainly generated under the anode bottom surfaces as a result of electrochemical reactions.[1] Then they move horizontally and upward to the top surface of the electrolyte, consisting of complex gas–liquid two-phase flows driven by both the anodic gas and electromagnetic forces (EMFs). Meanwhile, different sized-bubbles show some typical bubble mesoscopic dynamic characteristics, such as nucleation, growth, coalescence, and breakup phenomenon. Both of the above two physical phenomena have an important influence on the overall thermal balance and alumina mixing and distributions, as well as on the cell design, operational efficiency, and energy saving.[2] Therefore, further research of such key issues is beneficial for the efficient design and scale-up of the electrolysis reactors.

In the past few decades, there has been significant development related to the design, operation, scale-up, and application of the industrial test to the industrial-production cells. Nevertheless, some key technologies are waiting to be further studied because of the complex flows and bubble distributions and their unknown behavior under different sets of design and operating conditions. So far, the design and optimum operation of these electrolysis reactors have been primarily based on empiricism. For a reliable design, it is desirable to understand and obtain detailed two-phase flow distributions.

It is almost impossible to conduct the industrial measurements in real cells as a result of the high temperature and hostile environment. Therefore, both the experimental and simulation approaches have been extensively performed.[3–8] The experimental approach mainly includes small-scale, high-temperature electrolytic models[3,4] and both large-

(Published online November 2, 2017)

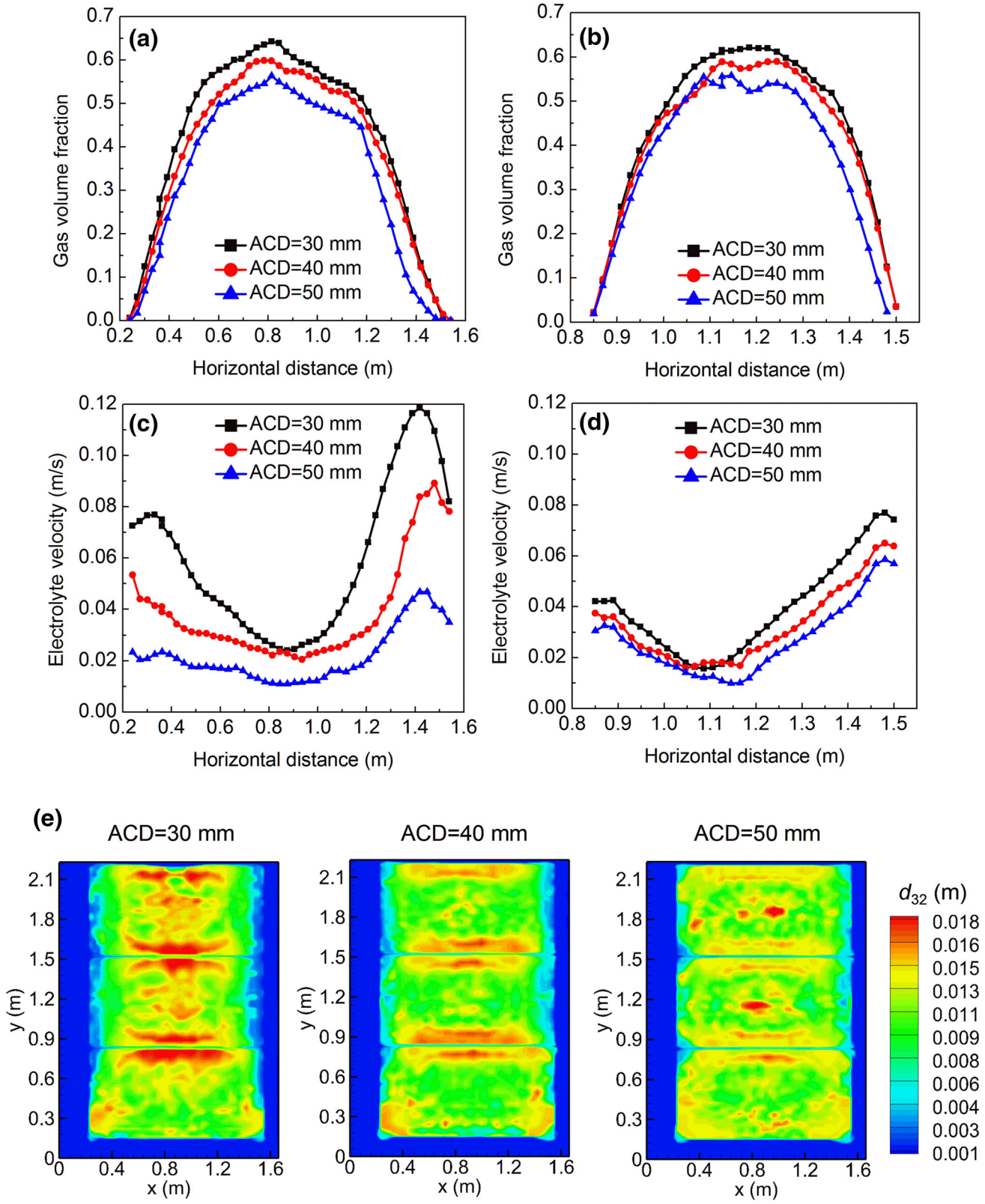

Fig. 1. Effect of ACD on the simulated results: (a–b) gas volume fraction, (c–d) electrolyte velocity, and (e) BSD.

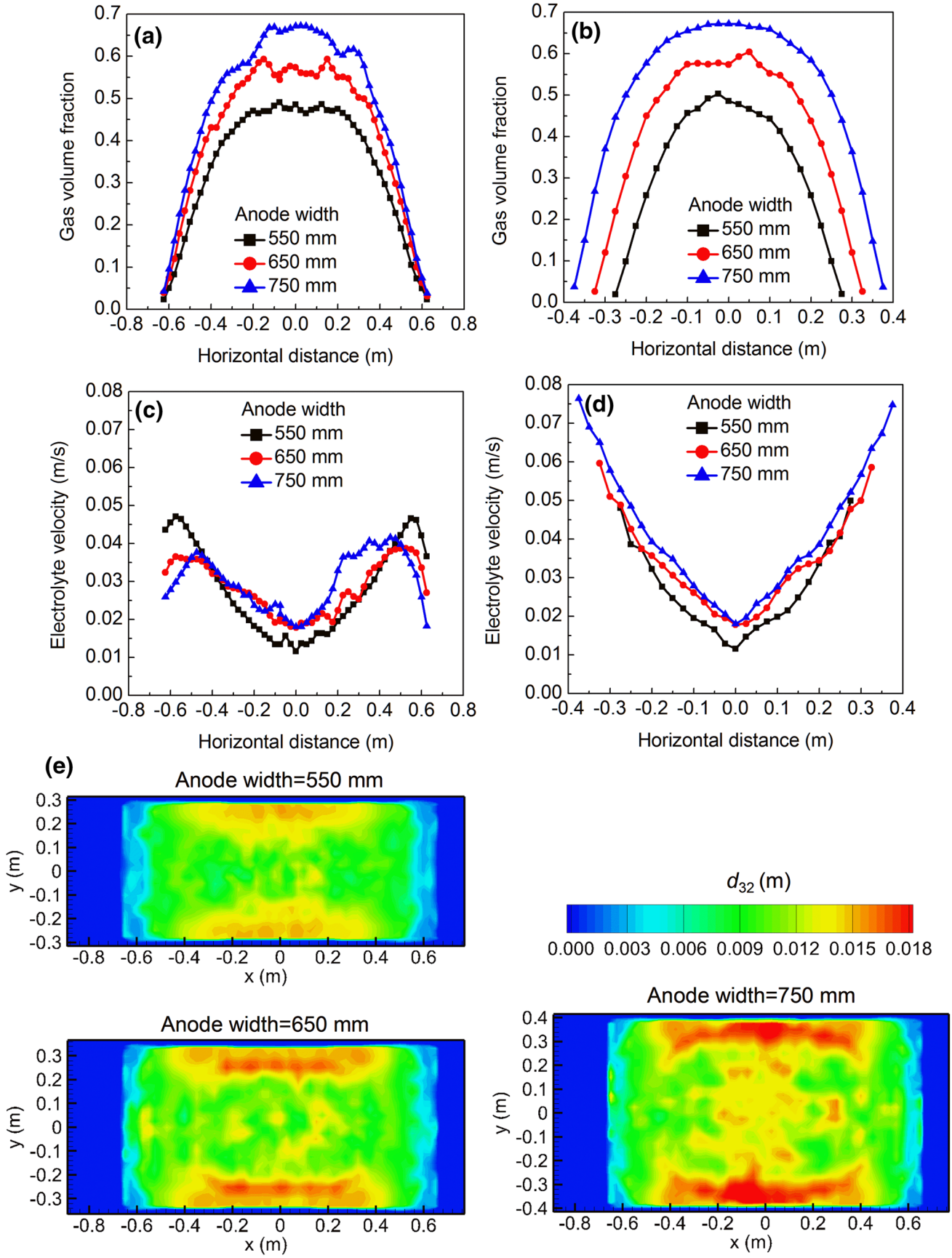

Fig. 2. Effect of anode width on the simulated results: (a–b) gas volume fraction, (c–d) electrolyte velocity, and (e) BSD.

scale, air–water[5,6] and low-temperature electrolytic models.[7,8] As demonstrated in these experimental investigations, although many of the mesoscopic bubble dynamic behaviors and macroscopic flow patterns have been obtained, some key issues and the relevant affecting factors remain somewhat limited because of the descriptive information or qualitative analysis resulting from restriction on the various experimental conditions, especially for the regions under the anode bottom.

As an alternative, the computational fluid dynamics (CFD) has been proved to be a powerful tool for the performance prediction, design, and scale-up of cells. Specifically, the well-known Euler–Euler model is favored to model and evaluate the gas–liquid flows in cells.[9–12] Most of the earlier simulations of gas–liquid, two-phase flows were focused on the bulk flow properties. A more detailed review of these investigations is given in our previous work,[13] and the reasonable closure of the two-fluid approach depends heavily on the appropriate selection of interphase forces, turbulence, and bubble size distribution (BSD). As a result of lack of experimental data for validation, most CFD predictions only considered drag force, standard k–ε model, and a constant bubble diameter.[9–12,14] Encouragingly, more systematic investigations were conducted by Feng et al.[15] based on the innovative experiment framework implemented by Cooksey and Yang.[6] Nevertheless, the strict prediction performance of different interphase forces and turbulence models has not been quantified or characterized adequately. Thus, the detailed effects of the above two key elements have been investigated systematically by Zhan et al.,[16] and a good quantitative agreement with the reliable experimental data has been obtained. Moreover, the further numerical simulations of coupling behavior of bubble distribution characteristics and overall two-phase flows have been originally presented based on a coupled computational fluid dynamics-population balance model (CFD-PBM) in our recent work.[17] The well-validated macroscopic gas–liquid flows and more acceptable bubble distribution characteristics within cells, especially in the anode–cathode distance (ACD) regions, have been predicted by considering appropriate bubble coalescence and breakup mechanisms. The detailed CFD-PBM coupled model and its widespread applications can be referred to the available literatures.[18,19] It should be noted, however, that the effect of varying different cell design and operating conditions on both the hydrodynamics and BSDs has not been addressed in the open literature extensively.

Based on the former progress and confirmed reliability of the CFD-PBM coupled approach, the objective of this work is to investigate the effects of different cell design and operating parameters on the gas–liquid, two-phase flows and bubble distribution characteristics in aluminum electrolysis cells. The influence of bubble breakup behavior is also discussed and compared in the simulated results in the ACD regions. This would help to better understand some of the design and scale-up considerations for the modern aluminum electrolysis cell.

MODEL DESCRIPTION AND SIMULATION DETAILS

Computational Fluid Dynamics-Population Balance Model Coupled Description

Based on our prior numerical exercises,[16,17] the numerical simulations are carried out using a 3D CFD-PBM coupled model. The CFD model is used to investigate the bulk gas–liquid, two-phase flow fields and the PBM is proposed to model the BSDs by solving the population balance equation (PBE). The drag force with Grace correlation, turbulent dispersion force with Somonin correlation, dispersed standard k–ε model, a bubble-induced turbulence (BIT) model of Sato's eddy viscosity, and bubble coalescence and breakup mechanisms proposed by Luo and Svendsen[20,21] are considered. The coupling between the CFD and the PBM is achieved through the calculation of the bubble Sauter mean diameter d_{32}. The detailed model equations and descriptions, the coupling strategy, and algorithms can be found in our previous work,[16,17] and therefore, they are not shown here because of space limitations. The simulation details can be seen in the Supplementary Material.

RESULTS AND DISCUSSION

Based on our previous work,[16,17] the cell design and operating parameters similar to the experimental conditions were selected as the basis to perform different analyses. The details of the comparisons between the CFD-PBM simulations with and without bubble breakup process are presented and shown in the Supplementary Material (see supplementary Fig. S1). The overall and local comparisons for the gas–liquid flows and BSDs under the anode bottom regions will be presented and discussed. Since the overall two-phase flow patterns do not change significantly for different cell design and operating parameters, the qualitative comparisons of the basic flow patterns are not shown here and only the quantitative comparisons at a typical position (z = 0.03 m) for different cases are conducted. Note that it is not possible to run the simulation of an industrial operation cell for the current comparison and analysis. Therefore, the predicted results influenced by the EMFs for the two computational models are ignored.

Effect of Inter-Anode Channel Width

The predicted results along the length and width centerlines of Anode-B2 for three different inter-anode channel widths and the detailed discussion can be seen in the Supplementary Material (see supplementary Fig. S2).

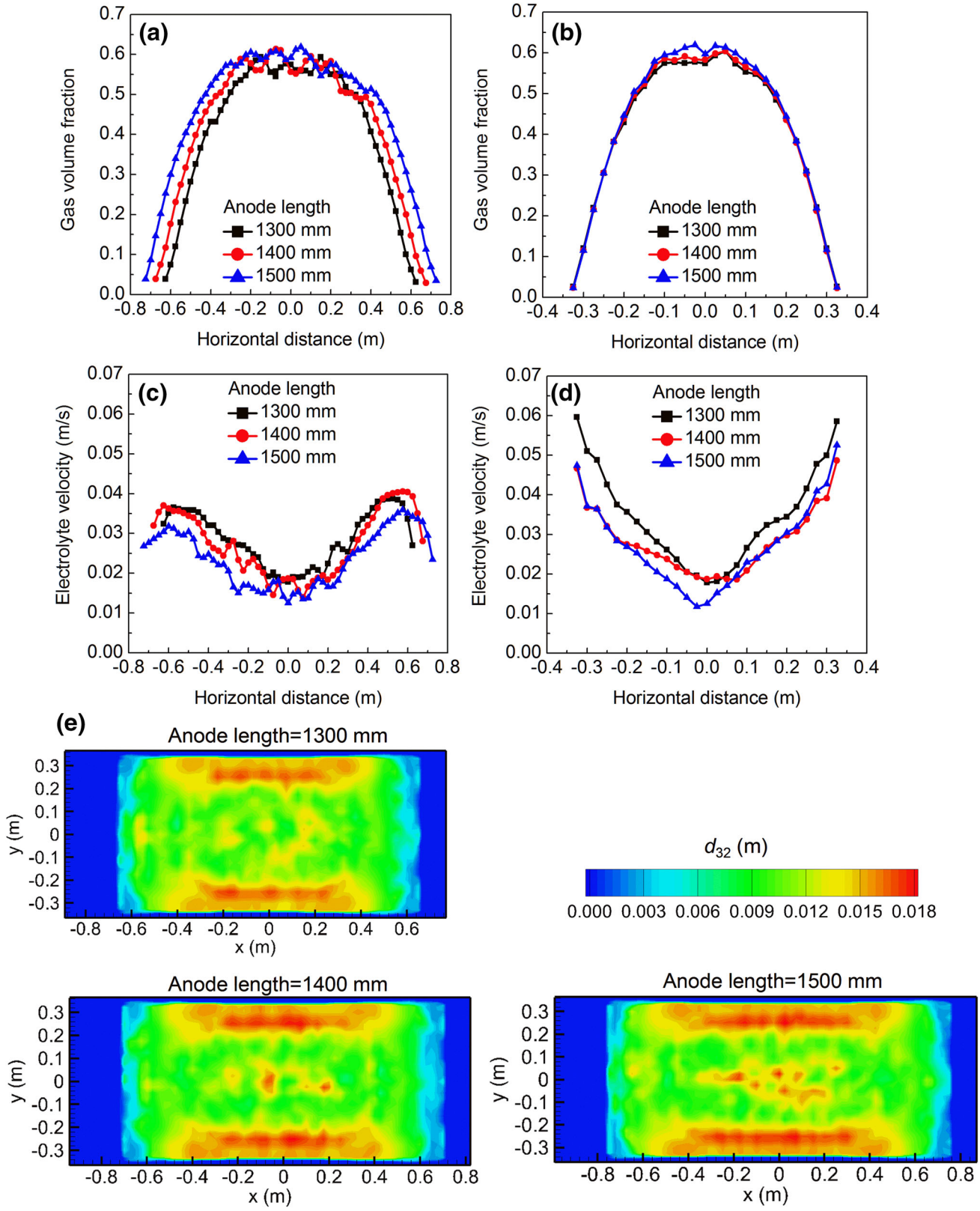

Fig. 3. Effect of anode length on the simulated results: (a–b) gas volume fraction, (c–d) electrolyte velocity, and (e) BSD.

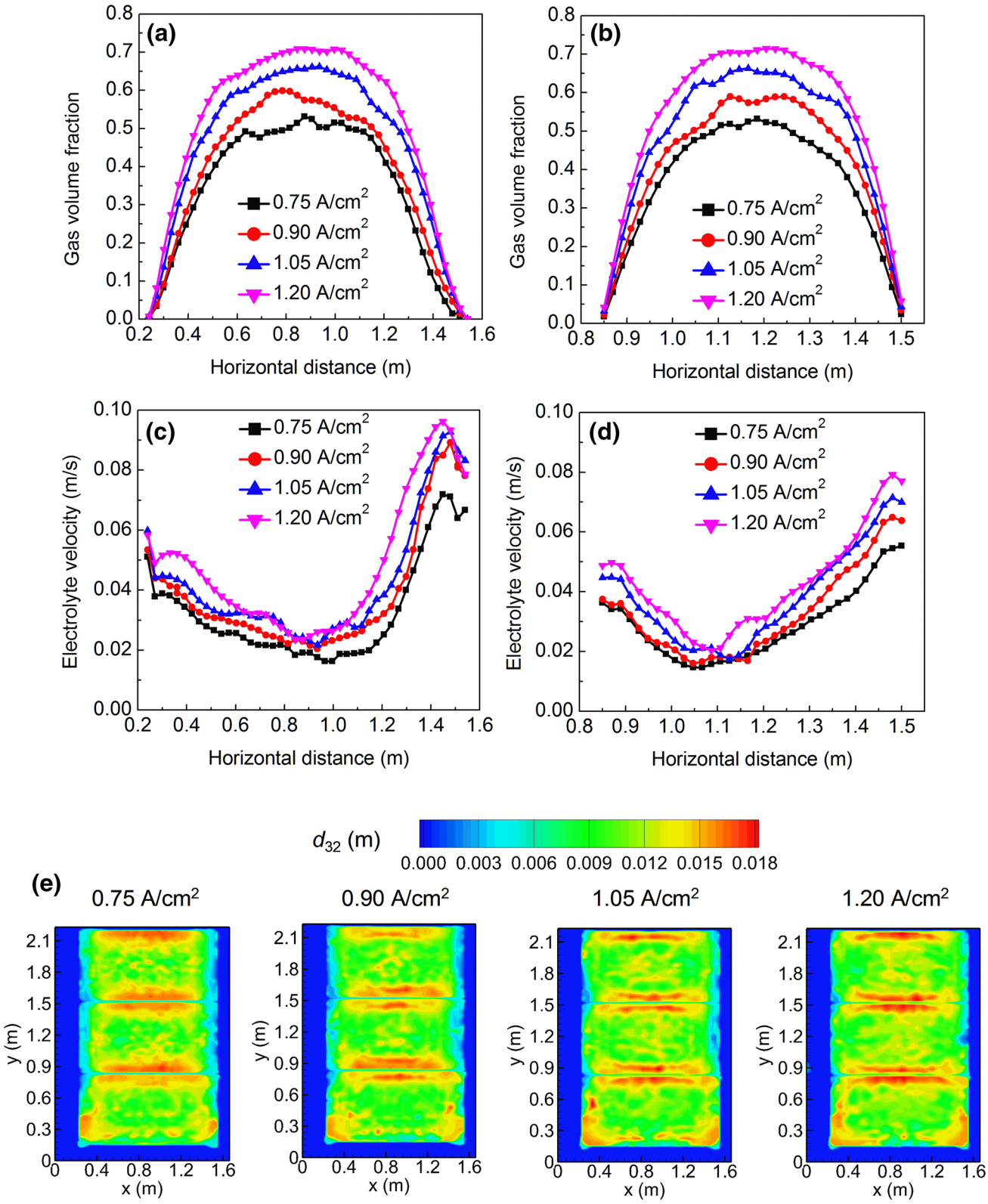

Fig. 4. Effect of current density on the simulated results: (a–b) gas volume fraction, (c–d) electrolyte velocity, and (e) BSD.

Effect of Anode—Cathode Distance

The simulation results for three different ACDs are shown in Fig. 1. Generally, with decreasing ACD, the gas volume fraction increases along both centerlines. The main reason is that there is a smaller electrolyte volume available in the anode–cathode space with smaller ACDs, and consequently, it may cause difficulties for the bubble movement inside the electrolyte domain. In other words, the gas velocity can be actually lower. Also, the volume of the generated gas bubbles remains the same at a given current density for different cases. Therefore, the gas volume fraction would certainly increase with decreasing ACD. The electrolyte velocity would also increase. A possible reason is that the momentum exchange is enhanced and the liquid energy dissipation caused by the anode gas evacuation should decrease.

Figure 1e demonstrates that the larger bubbles can be observed in the boundary regions near the inter-anode channels with smaller ACDs. Meanwhile, although the bubbles become smaller as the ACD increases, the more uniform bubbles can be obtained. This is also mainly due to the higher gas volume fractions, as mentioned above, resulting in higher bubble coalescence rates.

Effect of Anode Width and Length

Different anode widths and lengths were considered and compared for the one-anode model as shown in Figs. 2 and 3. From Fig. 2, the gas volume fraction increases with increasing anode width along both centerlines and the trend is more obvious along the width centerline. This is because more bubbles are generated with increasing anode width and the bubbles have to travel a longer path. Therefore, more and more bubbles cannot effectively escape from the anode bottom regions, leading to an increase in the number of large bubbles. As a result, the predicted electrolyte velocity increases with increasing anode width in most regions as a result of the enhanced momentum exchange with higher gas volume fractions. Nevertheless, in the regions near the side and central channels, the electrolyte velocity appears to be an opposite trend, possibly as a result of the electrolyte backflow as stated before.

Figure 3 shows the gas volume fraction increases with increasing anode length along the anode length centerline, but it keeps nearly the same along the anode width centerline. The electrolyte velocity decreases as the anode length increases in most regions along both centerlines, and these present an opposite trend compared with the effects on the gas volume fractions. The main reason, however, may be that the electrolyte backflow can cause more turbulent energy to be dissipated, resulting in lower velocity magnitude.

Figures 2 and 3 also show that the bubble size increases with increasing anode width nearly in the whole regions but that it increases with increasing anode length in only a small part of central regions. As known, the bubble coalescence chance can be more obvious when increasing anode width because of the increase of gas volume fraction for the whole regions. Instead, since the gas volume fraction increases obviously only in the regions along the anode length centerline when increasing anode length, the bubble coalescence process can only be strengthened and it may keep nearly the same in other regions.

Effect of Current Density

The predicted results for different anode current densities are shown in Fig. 4. With increasing current density, the gas volume fraction increases. This is expected because the total amount of anode gas produced should be higher and is proportional to the current density based on Faraday's law, which means that more bubbles gradually accumulate under the anode bottom regions. As a result, the electrolyte velocity increases with increasing current density. The reason is that the bubble-driven electrolyte flows can be enhanced because of higher bubble-driven forces caused by bubble evolution with higher gas volume fractions.

Figure 4e indicates that the simulated current densities have no significant effect on the BSDs. This is may be because, on the one hand, the bubble coalescence rate may increase with increasing gas volume fraction at higher current density. On the other hand, however, more smaller sized bubbles are generated under the whole anode bottom surface based on the assumption that the size of all inlet-bubbles is 1 mm at the mass-flow-inlet boundary. If readers are interested in more details, please refer to our previous work.[17] Therefore, these two main factors together contribute to the similar BSDs from our current CFD-PBM simulations.

Effect of Electrolyte Depth

The supplementary Figure S3 illustrates the predicted results for different electrolyte depths. It is obvious from Fig. S3a that the gas volume fraction decreases with increasing electrolyte depth along the anode length centerline near the side channels. In addition, the gas volume fraction decreases slowly with increasing electrolyte depth mainly along the anode width centerline near the anode central regions (Fig. S3b). Nevertheless, the electrolyte velocity variation shows an opposite trend to that of the gas volume fractions along both centerlines (Fig. S3c and d). This is because more fluid space for the bubbles have to accelerate and to induce the electrolyte flows by the drag force

effect with larger electrolyte depth. Hence, the gas velocity can be increased and the bubbles can become smaller with larger electrolyte depths. The unexpected prediction can be attributed to the fact that the stronger electrolyte backflow from both the side and central channels to the ACD regions has a bigger effect than does the momentum exchange induced by the gas evacuation, especially for the larger electrolyte depth.

Figure S3e shows the simulated BSDs for different electrolyte depths. The bubble size becomes smaller as the larger electrolyte depths are used, especially in the anode edge regions near the inter-anode, side, and central channels. Obviously, the higher bubble coalescence rates from the higher gas volume fractions are just the main reason for such BSD characteristics.

CONCLUSION

The bubble breakup behavior has little effects on the gas–liquid, two-phase flows and BSDs under the anode bottom regions and hence can be ignored. The inter-anode channel width has no significant influence on the electrolyte velocity and gas volume fraction along the anode width centerline, while it has some differences along the anode length centerline. The predicted BSDs are nearly the same for different inter-anode channel widths. Both the gas volume fraction and the electrolyte velocity increase with decreasing ACD. The bubbles become smaller as the ACD increases and the more uniform bubbles can be obtained. With increasing anode width, the above simulation results increase in most of regions. When the anode length increases, the gas volume fraction increases along the anode length centerline and keeps nearly the same along the anode width centerline, while the electrolyte velocity decreases in most regions. The bubble size increases slightly with increasing anode length in only a small part of the central regions. With increasing current density, both the gas volume fraction and the electrolyte velocity increase, but the BSDs have little difference. With increasing electrolyte depth, the gas volume fraction decreases along the anode length centerline near the side channels and along the anode width centerline near the anode central regions, while the electrolyte velocity shows an obviously opposite trend. The bubble size becomes smaller with larger electrolyte depths, especially in the anode edge regions near the inter-anode, side, and central channels.

ACKNOWLEDGEMENTS

The authors are grateful for the financial support of the National Natural Science Foundation of China (51704126), the Natural Science Foundation of Jiangsu Province (BK20170551, BK20171301, BK20150511), the Natural Science Foundation of Higher Education Institutions of Jiangsu Province (17KJB450001), the Foundation of Senior Talent of Jiangsu University (2015JDG158), and the China Postdoctoral Science Foundation (2016M591781). Our special thanks are a result of anonymous reviewers for insightful suggestions on this work.

ELECTRONIC SUPPLEMENTARY MATERIAL

The online version of this article (https://doi.org/10.1007/s11837-017-2636-8) contains supplementary material, which is available to authorized users.

REFERENCES

1. Y.X. Liu and J. Li, *Modern Aluminum Electrolysis* (Beijing: Metallurgical Industry Press, 2008), pp. 3–8.
2. K.E. Einarsrud, I. Eick, W. Bai, Y.Q. Feng, J.S. Hua, and P.J. Witt, *Appl. Math. Model.* 44, 3 (2017).
3. R.G. Aaberg, V. Ranum, and K. Williamson, *Light Metals 1997*, ed. R. Huglen (Orlando, FL: TMS, 1997), pp. 341–346.
4. Z.B. Zhao, Z.W. Wang, B.L. Gao, Y.Q. Feng, Z.N. Shi, and X.W. Hu, *Metall. Mater. Trans. B* 47, 1962 (2016).
5. K. Vekony and L.I. Kiss, *Metall. Mater. Trans. B* 41, 1006 (2010).
6. M.A. Cooksey and W. Yang, *Light Metals 2006*, ed. T.J. Galloway (San Antonio, TX: TMS, 2006), pp. 359–365.
7. Y.Q. Xue, N.J. Zhou, and S.Z. Bao, *Chin. J. Nonferrous Met.* 16, 1823 (2006).
8. M. Alam, W. Yang, K. Mohanarangam, G. Brooks, and Y.S. Morsi, *Metall. Mater. Trans. B* 44, 1155 (2013).
9. Y.Q. Feng, M.A. Cooksey, and M.P. Schwarz, *Light Metals 2007*, ed. M. Sørlie (Orlando, FL: TMS, 2007), pp. 339–344.
10. Y.Q. Feng, W. Yang, M.A. Cooksey, and M.P. Schwarz, *J. Comput. Multiph. Flows* 2, 179 (2010).
11. J. Li, Y.J. Xu, H.L. Zhang, and Y.Q. Lai, *Int. J. Multiph. Flow* 37, 46 (2011).
12. S.Q. Zhan, M. Li, J.M. Zhou, J.H. Yang, and Y.W. Zhou, *J. Cent. South Univ. Technol.* 22, 2482 (2015).
13. S.Q. Zhan (Ph.D. Dissertation, Central SouthUniversity, Changsha, 2015).
14. Q. Wang, B.K. Li, and N.X. Feng, *Metall. Mater. Trans. B* 45, 272 (2014).
15. Y.Q. Feng, M.P. Schwarz, W. Yang, and M.A. Cooksey, *Metall. Mater. Trans. B* 46, 1959 (2015).
16. S.Q. Zhan, J.H. Yang, Z.T. Wang, R.J. Zhao, J. Zheng, and J.F. Wang, *JOM* 69, 1589 (2017).
17. S.Q. Zhan, Z.T. Wang, J.H. Yang, R.J. Zhao, C.F. Li, J.F. Wang, and J.M. Zhou, *Ind. Eng. Chem. Res.* 56, 8649 (2017).
18. S.C.P. Cheung, G.H. Yeoh, and J.Y. Tu, *AIChE J.* 54, 1689 (2008).
19. X.F. Liang, H. Pan, Y.H. Su, and Z.H. Luo, *Chem. Eng. Res. Des.* 112, 88 (2016).
20. H. Luo, Ph.D. Dissertation (Norwegian Institute of Technology, Trondheim, 1993).
21. H. Luo and H.F. Svendsen, *AIChE J.* 42, 1225 (1996).